

## 1 Atomic-Scale Andreev Probe of Unconventional Superconductivity

2 Wonhee Ko,<sup>1</sup> Sang Yong Song,<sup>1</sup> Jiaqiang Yan, Jose L. Lado, and Petro Maksymovych\*Cite This: <https://doi.org/10.1021/acs.nanolett.3c02658>

Read Online

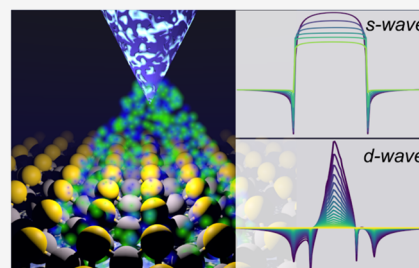
ACCESS |

Metrics &amp; More

Article Recommendations

Supporting Information

3 **ABSTRACT:** Recent emergence of low-dimensional unconventional superconductors  
 4 and their exotic interface properties calls for new approaches to probe the pairing  
 5 symmetry, a fundamental and frequently elusive property of the superconducting  
 6 condensate. Here, we introduce the unique capability of tunneling Andreev reflection  
 7 (TAR) to probe unconventional pairing symmetry, utilizing the sensitivity of this  
 8 technique to specific Andreev reflections. Specifically, suppression of the lowest-order  
 9 Andreev reflection due to quantum interference but emergence of the higher-order  
 10 Andreev processes provides direct evidence of the sign-changing order parameter in the  
 11 paradigmatic FeSe superconductor. TAR spectroscopy also reveals two superconducting  
 12 gaps, points to a possibility of a nodal gap structure, and directly confirms that  
 13 superconductivity is locally suppressed along the nematic twin boundary, with preferential and near-complete suppression of the  
 14 larger energy gap. Our findings therefore enable new, atomic-scale insight into microscopic, inhomogeneous, and interfacial  
 15 properties of emerging quantum materials.



16 **KEYWORDS:** *Andreev reflection, unconventional superconductivity, sign-changing gap, tunneling, quantum interference*

17 **T**he superconducting order parameter is a fundamental  
 18 quantum mechanical quantity directly related to the  
 19 pairing interaction that couples charges to form Cooper pairs.  
 20 In the standard Bardeen–Cooper–Schrieffer theory, which  
 21 describes most conventional metallic superconductors such as  
 22 tin and lead, the pairing potential is always attractive and  
 23 isotropic in space, with a corresponding order parameter being  
 24 isotropic and of the same sign in momentum space.<sup>1,2</sup> By  
 25 contrast, since the discovery of cuprate superconductors, many  
 26 materials exhibit anisotropic, sign-changing, chiral, and other  
 27 more complicated structures of the order parameter,<sup>3</sup> which  
 28 signifies the involvement of unconventional mechanisms for  
 29 superconductivity, including possible magnetic,<sup>4</sup> nematic,<sup>5,6</sup>  
 30 and charge order fluctuations.<sup>7,8</sup>

31 Identification of the order parameter symmetry is a  
 32 notoriously challenging problem for any new superconductors  
 33 and even for established superconductors of very high-quality  
 34 bulk crystals. In the example of iron chalcogenides, which is the  
 35 model material for the present study, the question of  
 36 fundamental pairing symmetry continues to be debated even  
 37 in the parent, single crystals of FeSe.<sup>9,10</sup> In fact, s-wave and d-  
 38 wave as well as mixed symmetries of the order parameter (e.g.,  
 39 s + id) have been proposed for FeSe depending on the specific  
 40 theoretical or experimental techniques.<sup>11–17</sup> Meanwhile, the  
 41 relatively small coherence length of most of the unconventional  
 42 superconductors, typically in the few nanometers range, raises  
 43 a further challenge to not only determine the averaged order  
 44 parameter symmetry but also to reveal its likely variations in  
 45 real space. Furthermore, spatially varying superconducting  
 46 properties form the foundation of many proposals for future

47 computing functionalities with exotic boundary states and  
 48 interfaces.<sup>18,19</sup>

49 A promising path to direct measurement of unconventional  
 50 superconductivity down to the atomic scale emerges from the  
 51 phenomenon of Andreev reflection. In Andreev reflection, the  
 52 electron crossing a metal–superconductor interface is reflected  
 53 as a hole, while a Cooper pair is injected into the  
 54 superconductor.<sup>20</sup> The corresponding excess current due to  
 55 Andreev reflection is the basis of the point-contact Andreev  
 56 reflection (PCAR) methodology which provided crucial  
 57 evidence in support of the d-wave pairing symmetry in cuprate  
 58 superconductors.<sup>21–23</sup> PCAR can also, at least in principle,  
 59 differentiate between different symmetries proposed for  
 60 FeSe,<sup>24</sup> and it was demonstrated to provide direct evidence  
 61 of the existence of two superconducting gaps.<sup>25–27</sup> The  
 62 minimum requirement for having just a single metal–super-  
 63 conductor contact implies that this technique can in principle  
 64 be shrunk to the atomic scale. However, the specificity of  
 65 PCAR to the structure of the order parameter originates from  
 66 momentum conservation across the so-called directional  
 67 contacts to the superconductor interface.<sup>24</sup> Reducing the size  
 68 of the contact to the atomic scale will remove momentum  
 69 resolution due to the Heisenberg uncertainty principle,<sup>69</sup>

**Received:** July 17, 2023

**Revised:** August 21, 2023

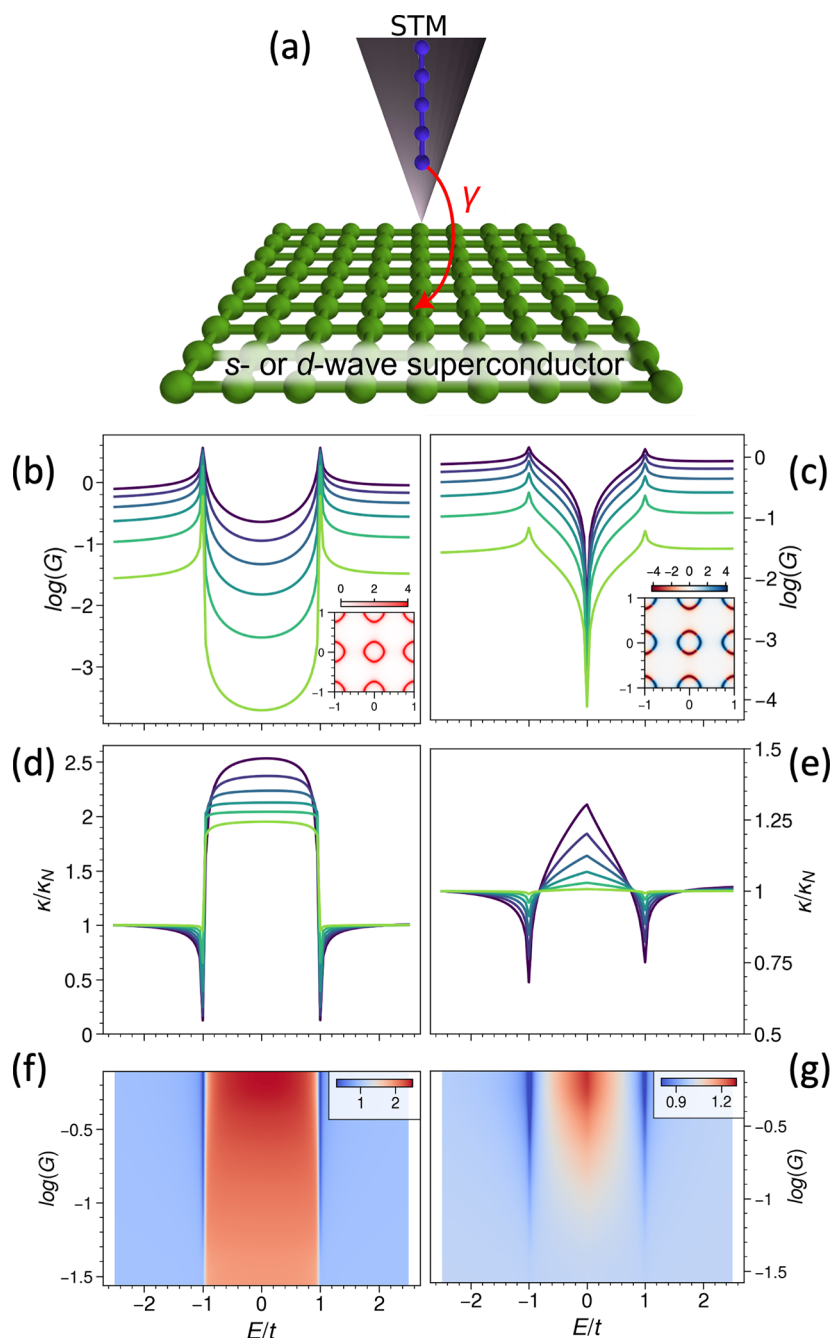


**Figure 1.** Illustration of the methodology of tunneling Andreev reflection (TAR) and its ability to differentiate superconducting order parameters. (a) Schematic of the transport setup used in the tight-binding modeling of TAR. (b,c) Conductance spectra for s-wave and d-wave order parameters as a function of tunneling barrier transparency  $\gamma = 0.1$  (light green) to  $0.6$  (dark blue). Insets show the corresponding Fermi surfaces. The superconducting gap persists qualitatively unchanged across the whole range of  $\gamma$ . (d,e) The corresponding renormalized decay rate ( $\kappa/\kappa_N$ ) spectra for the two order parameters. The onset of higher-order Andreev reflection is marked by  $\kappa/\kappa_N > 2$  for the s-wave and  $\kappa/\kappa_N > 1$  for the d-wave, providing key evidence to differentiate between the two symmetries in experiments. (f,g) Color maps of the decay rate spectra in panels d and e, respectively, as a function of conductance  $\log(G)$  (y axis) and energy  $E/t$  (x axis).

70 necessitating new approaches to both detect and quantify  
71 Andreev reflection with increasing spatial resolution.

72 In this paper, we present the first measurements of tunneling  
73 Andreev reflection (TAR) from an unconventional super-  
74 conductor. The TAR methodology detects Andreev reflection  
75 from the superconductor across an atomic-scale tunnel  
76 junction. It therefore strongly benefits from a precisely tunable  
77 transparency of the tunneling junction, and it uniquely probes  
78 higher-order Andreev reflection processes.<sup>28</sup> However, because

of atomic-scale dimensions, Andreev reflection is not  
momentum-resolved in TAR. Here, we reveal that this  
technique provides a unique signature of an unconventional  
order parameter. Specifically, the lowest order, single Andreev  
reflection is proportional to the expectation value of the  
superconducting gap across the Brillouin zone and therefore  
reflects the average value of the phase. Our measurements then  
unequivocally demonstrate the sign-changing nature of the  
superconducting order parameter in FeSe, due to nearly

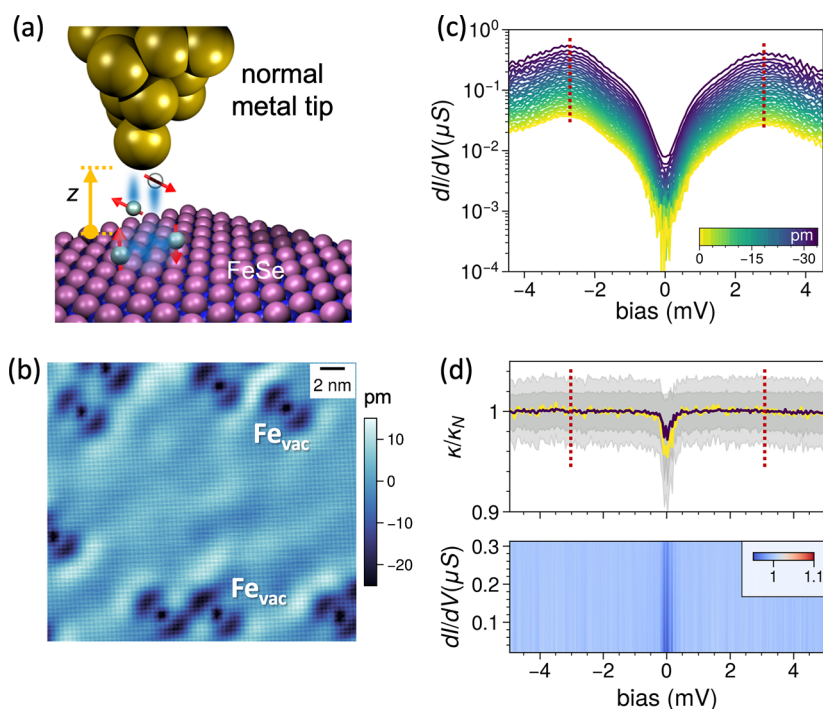


**Figure 2.** Schematic of experimental measurement of tunneling Andreev reflection. (a) Experimental setup for conductance and decay rate spectra. The spectra are measured between a metal tip and superconducting FeSe as a function of varying tunneling conductance controlled by tip-surface separation  $z$ . (b) STM image of an atomically flat FeSe surface with naturally occurring Fe vacancies (set point at  $V = -10$  mV,  $I = 50$  pA). (c) Superconducting gap spectroscopy as a function of  $z$  from 0 to  $-34$  pm (negative values toward the surface). (d) Decay rate spectra obtained from c and its corresponding color map view (bottom half). Within the error bars (gray area),  $\kappa/\kappa_N$  equals unity across the whole superconducting gap, directly witnessing the presence of sign-changing order parameter. The error bars were estimated from Bayesian fitting of the second-order polynomial function to the  $z$ -dependency of  $dI/dV$  at each tunneling energy in c. Red dashed lines mark the approximate edges of the superconducting gap.

88 complete suppression of the lowest-order reflection. Mean-  
 89 while, higher-order reflections persist. They further ascertain  
 90 the existence of two superconducting gaps in FeSe and point to  
 91 the possibility of a nodal  $d_{x^2-y^2}$  order parameter. Finally, we  
 92 demonstrate that the outer gap component is nearly  
 93 completely suppressed while approaching the twin boundary  
 94 in FeSe, explaining their preferential role as vortex pinning  
 95 centers.<sup>29–31</sup> TAR thus provides much needed direct evidence  
 96 for an unconventional superconducting order parameter, and it  
 97 also naturally complements several existing microscopy  
 98 techniques such as tunneling spectroscopy and quasiparticle  
 99 interference microscopy. In particular, the TAR provides true  
 100 atomic resolution. By contrast, quasiparticle interference  
 101 microscopy, extensively developed in both cuprates<sup>32–34</sup> and  
 102 iron-based superconductors,<sup>35–37</sup> is resolution limited to at  
 103 least tens of nanometers due to reconstruction of the scattering  
 104 properties in momentum space.

105 The experimental observable assumed by TAR—the decay  
 106 rate of tunneling conductance—principally differentiates the  
 107 technique from the conventional Andreev spectroscopy  
 108 including its proposed extension toward STM,<sup>38</sup> all of which  
 109 rely on the value of conductance itself. The decay rate  
 110 fundamentally enables selective detection of the lowest and  
 111 higher-order Andreev reflections.<sup>28</sup> Subsequently, the depend-  
 112 ence of Andreev reflection on the transparency of the tunneling  
 113 junction can be measured by TAR and directly compared to a  
 114 variety of theoretical models directly. By contrast, in point-  
 115 contact measurements, the transparency is generally a fixed and  
 116 unknown experimental value, which dramatically complicates  
 117 the degree by which pairing symmetry can be inferred.<sup>24,39</sup>

To illustrate the fundamental aspects of TAR, we first  
 present tight-binding simulations of the TAR (Figure 1a). The  
 tunneling conductance of a metal-superconductor contact is  
 calculated as a function of transmission coefficient  $\gamma$  for  
 Bogoliubov-de-Gennes Hamiltonians of the s-wave (Figure 1b)  
 and d-wave pairing (Figure 1c). Andreev reflection is detected  
 via a renormalized decay rate of tunneling conductance  $\kappa/\kappa_N$   
 (Figure 1d–g),<sup>28</sup> where  $\kappa_N$  is the decay rate at energies larger  
 than the superconducting gap. This choice of normalization  
 reduces the effect of unknowns in both calculations and  
 experiments, making  $\kappa/\kappa_N$  well-suited for theory-experiment  
 comparison.

For a conventional s-wave superconductor, the tunneling  
 current within the superconducting gap is fully suppressed at  $T$   
 = 0 K, except for Andreev reflection, as shown in Figure 1b. At  
 a small tunneling conductance, the decay rate due to the  
 Andreev current is twice that of the normal current at the  
 Fermi level. The superconducting gap is then registered by a  
 characteristic 1 to 2 transition of  $\kappa/\kappa_N$  across the gap, as shown  
 in Figure 1d. However, the maximum value of  $\kappa/\kappa_N$  itself  
 depends on the tunneling conductance, increasing beyond 2  
 when  $\gamma > 0.3$  (Figure 1d,f). This increase in  $\kappa/\kappa_N$  signals  
 higher-order Andreev reflections. Its additional signature is that  
 $\kappa/\kappa_N < 1$  (resonant enhancement) at the edges of the gap as  
 shown in Figure 1d. The conceptual origin of the higher-order  
 processes can be rationalized by considering tunneling contact  
 perturbatively, i.e., the dependency of tunneling conductance  
 on increasing powers of the transmission coefficient  $\gamma$ . Under  
 the conditions of weak coupling (small  $\gamma$ ), only the lowest-  
 order terms will contribute to the tunneling conductance, 147

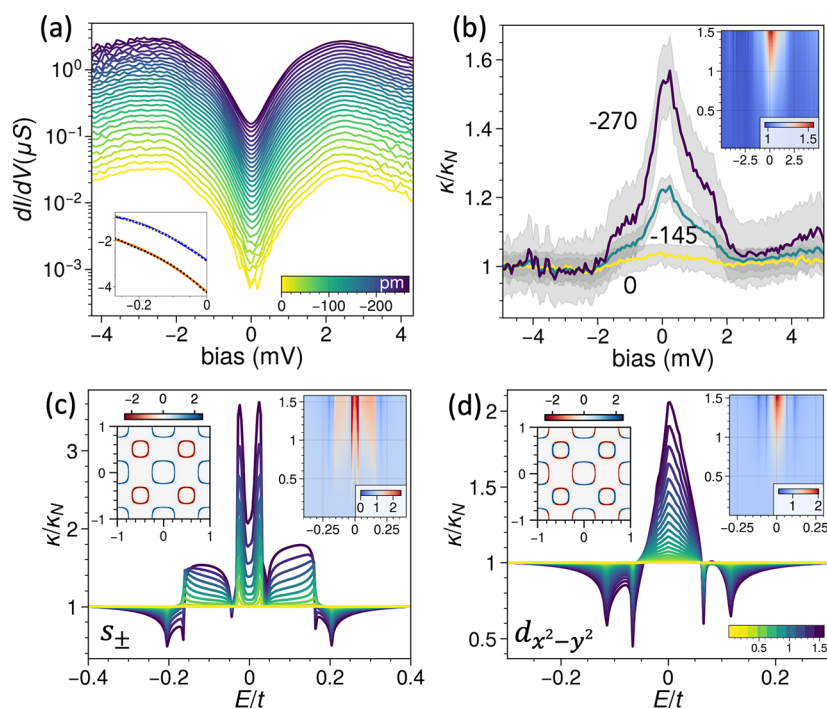


**Figure 3.** Emergence of higher-order Andreev reflection at increased tunneling conductance. (a) Measured  $dI/dV$  spectra as a function of decreasing  $z$  by up to  $-270$  pm. The inset shows individual  $z$ -dependency ( $x$  axis) of  $dI/dV$  ( $y$  axis) measured at energies of  $0$  mV (red) and  $-2$  mV (blue). (b) Decay rate spectra extracted from (a) at  $0$ ,  $-140$ , and  $-270$  pm. Higher-order Andreev reflection emerges as a zero bias peak with a maximum  $\kappa/\kappa_N$  value of  $1.6$ . The color map inset clearly shows the transition from suppressed to finite Andreev reflection as the tunneling conductance increases. (c,d) Tight-binding modeling of higher-order Andreev reflection for  $s_{\pm}$  and  $d_{x^2-y^2}$  order parameters with a two-gap structure. The colors of individual spectra correspond to tunneling transparency  $\gamma$  changing from  $0.01$  to  $1.5$ . The insets show the Fermi surface (left) and color map (right) of decay-rate spectra, with regions of higher-order reflection marked by  $\kappa/\kappa_N > 1$  (pink and red).

148 which corresponds to single-electron tunneling ( $\alpha\gamma$ ) and two-  
 149 particle Andreev reflection ( $\alpha\gamma^2$ ) in normal and super-  
 150 conducting states, respectively. However, when the tunneling  
 151 coupling increases, the value of higher-order Andreev reflection  
 152 terms (e.g.,  $\alpha\gamma^4$ ) becomes non-negligible, and this is directly  
 153 reflected in the value of  $\kappa/\kappa_N$  increasing beyond  $2$ . Note that in  
 154 contact measurements, all processes up to infinite order  
 155 contribute to tunneling conductance.<sup>40</sup> The ability to  
 156 selectively probe the lowest and at least a second order  
 157 reflection is a unique capability of TAR.

158 For a sign-changing d-wave order parameter with a nodal  
 159 gap, TAR spectroscopy is qualitatively different (Figure 1c,e).  
 160 The nodal quasiparticle tunneling completely suppresses the  
 161 lowest-order Andreev reflection, which is seen as  $\kappa/\kappa_N = 1$   
 162 across the gap at  $\gamma = 0.1$  (Figure 1e). However, the  
 163 contribution of higher-order Andreev reflection still emerges  
 164 with increased tunneling conductance.  $\kappa/\kappa_N$  becomes  
 165 enhanced in the middle of the gap and again suppressed at  
 166 the gap edges (Figure 1e,g). The net result is a central peak  
 167 structure with height rapidly increasing with an increased  
 168 tunneling conductance. Therefore, the combination of lowest  
 169 and higher-order Andreev reflections enables a robust test for  
 170 superconductivity as well as indirect but accessible information  
 171 about the order parameter symmetry.

172 FeSe continues to attract significant attention due to the  
 173 enhanced superconducting transition temperature  $T_c$  in the  
 174 electron-doped FeSe,<sup>41,42</sup> single-layer FeSe/SrTiO<sub>3</sub>,<sup>43,44</sup> and  
 175 the connection of this parent material to possible topological  
 176 superconductivity in FeSe<sub>0.5</sub>Te<sub>0.5</sub>.<sup>45,46</sup> Figure 2a shows a  
 177 schematic of the TAR experiment applied to FeSe. The  
 178 transparency of the contact is controlled by varying the

separation between the metal tip and FeSe surface (Figure 2b).  
 The  $\kappa/\kappa_N$  spectra are obtained from  $z$ -dependent tunneling  
 spectra of the superconducting gap (Figure 2c) as described in  
 ref 28. There are two questions posed for TAR: (1) Does  $\kappa/\kappa_N$   
 exceed unity across the gap? And (2), are there signatures of  
 the higher-order Andreev reflections? Note that the crossover  
 value of  $z$  to higher-order Andreev reflection is not known a  
 priori, and it will depend on the exact tip configuration and  
 other parameters outside the experimental control.

Figure 2d shows the decay rate spectroscopy for the range of  
 tunneling conductances up to  $0.5 \mu\text{S}$  (measured at  $4.5$  mV  
 bias). As shown in Figure 2d,  $\kappa/\kappa_N$  maintains a value of  $1$   
 across the whole gap within the statistical uncertainty. The  
 error bars were obtained from Bayesian fitting of the second-  
 order polynomial to the  $z$ -dependence of  $dI/dV$ . This result is  
 qualitatively different from plateau of  $\sim 2$  observed in a  
 conventional superconductor (Figure 1d).<sup>28</sup> Suppression of  
 Andreev reflection in the tunneling regime already indicates  
 the high likelihood of a sign-changing gap structure, more  
 directly and complementary to tunneling spectroscopy.

Meanwhile, extending the measurements to  $2-3 \mu\text{S}$  begins  
 to notably grow  $\kappa/\kappa_N$  in the middle of the gap, developing a  
 peak-like structure with pronounced shoulders and a maximum  
 observed value of about  $1.6$  in the middle of the gap (Figure  
 3a,b). The experimental spectra of higher-order Andreev  
 reflection exhibit some expected amount of experimental  
 variability but maintain their overall shape, as shown in Figure  
 S1. Already at this stage, we can make a direct comparison to  
 the results of tight-binding modeling with the sign-changing  
 order parameter symmetries for FeSe (Figure S3), specifically  
 the extended s-wave shown in Figure 3c and the nodal d-wave 209

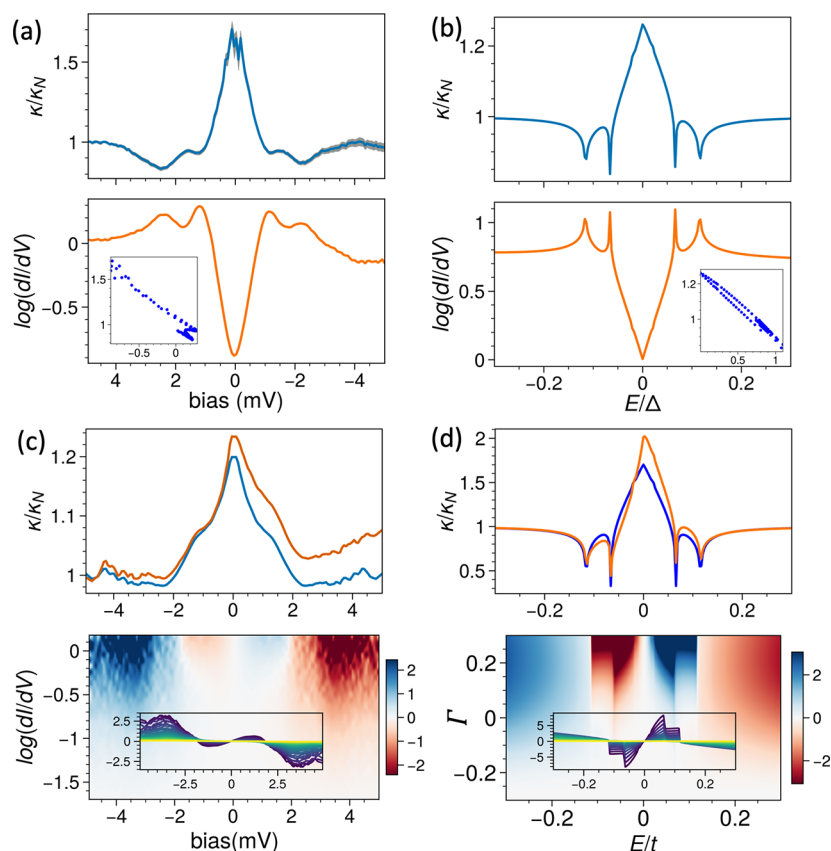


**Figure 4.** Comparison of measured and calculated decay rate spectra for the  $d_{x^2-y^2}$  order parameter. (a) Correspondence between measured decay rate spectra (top) and conductance spectra (bottom). Inset shows the nearly linear anticorrelation between them. (b) Similar comparison for the tight-binding model with a sign-changing order parameter, closely reminiscent of the measurements in panel a. (c) Asymmetry of decay rate spectra manifested by comparison between the decay rate spectrum measured at  $42 \mu\text{S}$  (orange) and its symmetrized form (blue, top panel). Bottom panel shows the asymmetry of the conductance spectra as a function of the tunneling conductance. The asymmetry is registered as a relative increase of the density of states below the Fermi level outside the superconducting gap and, oppositely, a relative decrease of the density of states within the superconducting gap region. (d) Tight-binding modeling that qualitatively reproduces all the asymmetries observed experimentally, both in the decay rate and conductance spectra.

210 in Figure 3d, calculated for the two-pocket Fermi surface  
211 consistent with FeSe.

212 The Fermi surface of FeSe constitutes hole Fermi pockets at  
213 the  $\Gamma$  point, and electron Fermi pockets at the M point (Figure  
214 S2).<sup>47–49</sup> For both order parameters, Andreev reflection is  
215 suppressed at small tunneling conductance (yellow lines in  
216 Figure 3c,d), in close agreement with Figure 2d. Notably, this  
217 is also true for the fully gapped  $s_{\pm}$  order parameter, where the  
218 nodal lines do not intersect with Fermi surface pockets. The  
219 Andreev signal, in this case, is suppressed because of  
220 destructive interference between opposite-signed pockets of  
221 the Fermi surface, which is uniquely probed by TAR.  
222 Meanwhile, calculations for both  $s_{\pm}$  and d-wave exhibit  
223 higher-order Andreev reflection, albeit with different spectral  
224 signatures. The experimental signal in Figure 3b exhibits a  
225 peak-and-shoulder structure concentrated around the middle  
226 of the gap, similar to the sign-changing d-wave order parameter  
227 in Figure 3d. The extended s-wave in Figure 3c exhibits a larger  
228  $\kappa/\kappa_N$  across the full width of the superconducting gap and even  
229 slight enhancement at the gap edges. It is worth noting that the  
230 average gap is zero when integrated in the Fermi surface for  
231  $d_{x^2-y^2}$  order, i.e.,  $\langle \Delta_{d_{x^2-y^2}}(\mathbf{k}) \rangle_{\text{FS}} = 0$ , whereas  $\langle \Delta_{s_{\pm}}(\mathbf{k}) \rangle_{\text{FS}} \neq 0$  for  
232  $s_{\pm}$  order. For the transport setup of our tight-binding  
233 modeling, this gap average determines the behavior of  $\kappa/\kappa_N$ ,  
234 accounting for the differences between the two orders.

Comparison with other superconducting orders is included 235  
in the Supporting Information (Figure S4). 236

Two additional characteristics of the higher-order Andreev 237  
reflection establish further agreement between modeling and 238  
experiment and also directly infer the two-gap superconducting 239  
structure. From the modeling results in Figures 1 and 3 and 240  
Figure S4,  $\kappa/\kappa_N$  is reduced below 1 (tunneling conductance is 241  
resonantly enhanced) at the superconducting gap edges. 242  
Although this effect is broadened by lifetime and thermal 243  
effects, we directly observed it in the decay rate spectroscopy 244  
on Pb(110).<sup>28</sup> On FeSe, particularly at large tunneling 245  
conductance, the conductance spectra clearly manifest the 246  
inner-gap structure, with gap positions at  $\pm 1.1$  meV (Figure 4a, 247 f4  
orange curve). The inner gap width is consistent with 248  
previously published results.<sup>26</sup> For the tunneling conditions 249  
corresponding to these spectra, the shoulder structure of 250  
higher-order Andreev reflection from Figure 3b becomes more 251  
pronounced, with now three clear peaks in  $\kappa/\kappa_N$  within the 252  
 $\pm 2.5$  meV range. Moreover, the dips separating these peaks 253  
coincide within measurement accuracy with the peaks in the 254  
 $dI/dV$  spectrum in near exact similarity to the simulated results 255  
in Figure 4b. The resonant enhancement is less pronounced in 256  
the experiment due to broadening effects. However, the 257  
observation directly points toward a two-gap structure of FeSe, 258  
confirming earlier results and providing another point of 259

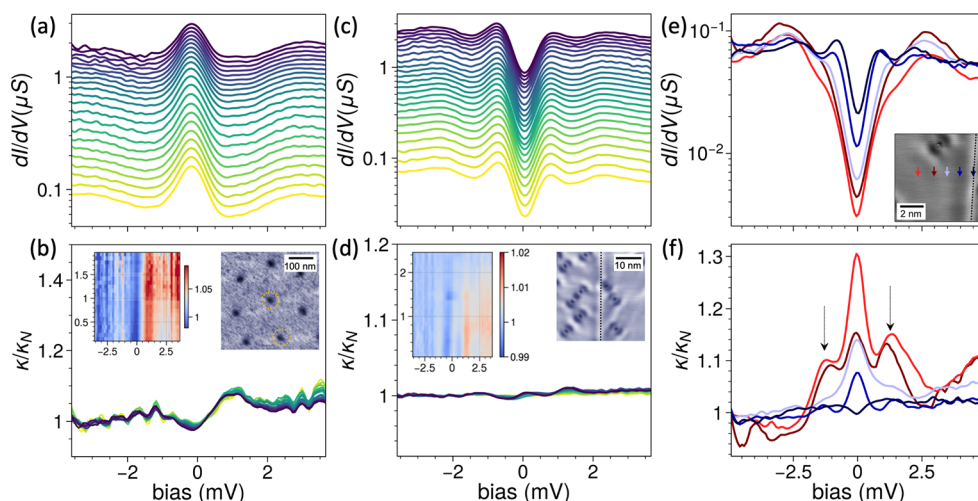


**Figure 5.** Tunneling Andreev reflection of topological defects on FeSe. Conductance spectra (a,c) and their corresponding decay rate spectra (b,d) acquired at the vortex center (a,b) and at the nematic twin boundary (c,d).  $\kappa/\kappa_N$  spectra remain essentially unity for both vortex and twin boundary. Insets of panel b and d show correspondingly the color maps of the decay-rate spectra (left) and the representative STM images of the surface areas of FeSe containing the topological defects (right; imaging set point bias =  $-2.5$  mV,  $I = 100$  pA for panel b; bias =  $-10$  mV,  $I = 50$  pA for panel d). The range of tunneling conductance probed for both entities is comparable to that for the bare surface in Figure 3b. (e,f) The evolution of conductance (e) and tunneling Andreev spectra (f) upon approaching the twin boundary. The zero bias conductance in e is dramatically increased, indicating suppression of superconductivity. Andreev spectra clearly reveal gradual suppression of the outer (via suppression of shoulders marked by arrows) as well as the inner gap (via suppression of the main peak). At present, the definitive conclusion as to whether the inner gap is fully suppressed inside the twin boundary is limited by the thermal broadening at 1.2 K.

260 agreement with respect to the higher-order Andreev reflection  
261 origin of experimentally measured  $\kappa/\kappa_N$ .

262 Another characteristic of the decay rate spectra is its  
263 asymmetry around the Fermi level, as shown in Figure 4c  
264 (orange line). In particular,  $\kappa/\kappa_N$  outside of the super-  
265 conducting gap (larger than 2.5 meV energy) is higher at  
266 energies above the Fermi level than below. This effect can be  
267 numerically confirmed by symmetrizing the measured  $dI/dV$   
268 around the Fermi level prior to calculating  $\kappa/\kappa_N$ , resulting in  
269 the blue line in Figure 4c. Note that the overall peak structure  
270 is not strongly affected. Figure 4c, bottom panel, also shows  
271 the asymmetric part of the  $dI/dV$  spectrum around the Fermi  
272 level, which gives rise to the asymmetry in  $\kappa/\kappa_N$ . The  
273 asymmetry is also observed in tight-binding simulations  
274 (Figure 4d). Here, the asymmetry of  $\kappa/\kappa_N$  directly stems  
275 from the asymmetry of the electronic structure in the normal  
276 state. Interestingly, this asymmetry in the spectra is manifested  
277 more strongly closer to the contact. This behavior can be  
278 readily rationalized from the perturbative point of view, where  
279 a small asymmetry in a low-order process  $\alpha(\omega)/\alpha(-\omega) \approx 1 -$   
280  $\epsilon$  becomes stronger for higher-order processes  $\alpha(\omega)^N/\alpha(-\omega)^N$   
281  $\approx 1 - N\epsilon$ .

282 The above measurements provide strong new evidence for  
283 the unconventional sign-changing superconducting order  
284 parameter in FeSe with two gaps around 1.1 and 2.5 meV  
285 energies. Moreover, TAR spectroscopy is more consistent with  
286  $d_{x^2-y^2}$  order parameter symmetry, rather than  $s_{\pm}$  within the  
287 accuracy of the present measurements and transport modeling.  
288 Reducing the broadening effects, for example, by measure-  
289 ments at progressively lower temperatures will help make this  
290 distinction even more clear in the future (Figure S5).

291 As an atomic-scale technique, TAR is uniquely poised to  
292 probe inhomogeneous and/or localized superconductivity. To  
293 this end, we measured Andreev spectra on an Abrikosov vortex  
294 and a nematic twin boundary (Figure 5). As the super-  
295 conducting order parameter is suppressed in the vortex center,

the value of  $\kappa/\kappa_N$  should be approximately 1, indicating weak  
energy dependence of normal tunneling in the  $\pm 2$  meV  
window around the Fermi level. The experimental decay rate  
spectra across the range of tunneling conductance comparable  
to those of Figures 2 and 3 indeed reveal a value that is very  
close to unity (Figure 5b). Meanwhile, the vortex-bound state  
is clearly observed in the  $dI/dV$  spectra (Figure 5a), which is  
perhaps responsible for the slight modulation of  $\kappa/\kappa_N$  around  
the Fermi level. For reference, the spectra of the normal state  
FeSe above the superconducting gap reveal hardly any features  
(Figure S1d), further ascertaining that the tunneling regime  
itself is robust and the analysis is largely free from numerical  
artifacts.

Meanwhile, the spectra from the twin boundaries also reveal  
no significant deviation of  $\kappa/\kappa_N$  from unity across the  
superconducting gap (Figure 5d), with no detectable  
signatures of lowest- or higher-order Andreev reflection  
(Figure 5d). The twin boundaries exhibit a narrower gap  
than the  $\pm 2.5$  meV value for the defect-free FeSe (Figure 5c).  
This is in agreement with prior works, where it was suggested  
that superconductivity is reduced but still present along the  
boundaries,<sup>29</sup> and may even be used as evidence of time-  
reversal symmetry breaking the order parameter.<sup>30</sup>

Figure 5e,f shows the evolution of conductance and Andreev  
spectra as the tip approaches the twin boundary. Conductance  
spectra are overall consistent with ref 30, showing suppression  
of the larger (2.5 meV) energy gap. Andreev spectra very clearly  
reveal this effect via suppression of the shoulders on the side of  
the main peak, Figure 5f. Meanwhile, the intensity of the main  
peak is also diminished on approaching the gap, approximately  
linearly correlating with the zero-bias conductance of the  
tunneling spectra. At present, we cannot further determine  
whether the suppression of Andreev current in the middle of  
the twin-boundary is due to thermal broadening effects on the  
much reduced inner gap at our lowest measurement temper-  
ature of 1.2 K or the more intrinsic quantum interference. The

332 residual gap-like feature in  $dI/dV$  spectra on twin boundaries  
333 (Figure 5c) was reported to be fully gapped below 0.4 K,<sup>30</sup>  
334 which would indicate that superconductivity is still present  
335 inside the twin. However, the twin boundary also acts as an  
336 extended defect, which may suppress the unconventional  
337 superconducting order in FeSe due to the pair breaking effect.  
338 Any type of local defect that creates momentum scattering will  
339 average out the sign-changing gap in reciprocal space, giving  
340 rise to in-gap modes that locally quench the superconducting  
341 order. This mechanism is analogous to the quenching of  
342 superconductivity in conventional superconductors by mag-  
343 netic impurities.<sup>50</sup> These data clearly reveal the ability of  
344 Andreev reflection to probe nanoscale variations of super-  
345 conductivity, enabling a more robust assignment of low-energy  
346 features in the tunneling spectra of superconductors. The  
347 nonsuperconducting twin boundary is also very consistent with  
348 it being the attractive region for superconducting vortices in  
349 FeSe.<sup>29–31</sup>

350 Here, we have presented the first measurements of tunneling  
351 Andreev reflection on an FeSe superconductor. The unique  
352 ability to probe both lowest- and higher-order Andreev  
353 reflections in tunneling measurements enables probing the  
354 order parameter symmetry and the two-gap structure while  
355 simultaneously having access to the local density of states from  
356 conductance spectroscopy and atomic-scale resolution. The  
357 probability for the lowest-order Andreev reflection is found to  
358 be proportional to the expectation value of the super-  
359 conducting gap across the Brillouin zone. The lowest-order  
360 Andreev reflection is suppressed on FeSe within the measure-  
361 ment accuracy, while higher-order processes reveal a character-  
362 istic peak-like shape with pronounced shoulders. Through a  
363 detailed comparison to tight-binding modeling, our results  
364 provide the first direct measurement of the sign-changing  
365 nature of the superconducting order parameter with atomic  
366 spatial resolution. The Andreev spectra also reveal clear  
367 suppression of the higher energy gap upon approaching the  
368 nematic twin boundary. Our measurements provide additional  
369 evidence to probe the fundamental origins of superconducting  
370 pairing in FeSe, and they set the stage for quantitative  
371 microscopic characterization of the phase diagram of FeSe as a  
372 function of doping and Te substitution. Furthermore, by taking  
373 advantage of the tunability of tunneling coupling, TAR enables  
374 new insight into pairing mechanisms of unconventional  
375 superconductors and is likely to provide valuable insight into  
376 emerging quantum materials, including exotic superconductiv-  
377 ity for quantum information science.

## 378 ■ ASSOCIATED CONTENT

### 379 **SI** Supporting Information

380 The Supporting Information is available free of charge at  
381 <https://pubs.acs.org/doi/10.1021/acs.nanolett.3c02658>.

382 Additional experimental data and modeling results for  
383 the tunneling Andreev reflection (PDF)

## 384 ■ AUTHOR INFORMATION

### 385 Corresponding Author

386 **Petro Maksymovych** – Center for Nanophase Materials  
387 Sciences, Oak Ridge National Laboratory, Oak Ridge,  
388 Tennessee 37831, United States; [orcid.org/0000-0003-0822-8459](https://orcid.org/0000-0003-0822-8459);  
389 Email: [maksymovychp@ornl.gov](mailto:maksymovychp@ornl.gov)

## Authors

**Wonhee Ko** – Center for Nanophase Materials Sciences, Oak  
Ridge National Laboratory, Oak Ridge, Tennessee 37831,  
United States; Department of Physics and Astronomy,  
University of Tennessee, Knoxville, Tennessee 37996, United  
States; [orcid.org/0000-0002-6155-1485](https://orcid.org/0000-0002-6155-1485)  
**Sang Yong Song** – Center for Nanophase Materials Sciences,  
Oak Ridge National Laboratory, Oak Ridge, Tennessee  
37831, United States  
**Jiaqiang Yan** – Materials Science and Technology Division,  
Oak Ridge National Laboratory, Oak Ridge, Tennessee  
37831, United States; [orcid.org/0000-0001-6625-4706](https://orcid.org/0000-0001-6625-4706)  
**Jose L. Lado** – Department of Applied Physics, Aalto  
University, 02150 Espoo, Finland

Complete contact information is available at:  
<https://pubs.acs.org/10.1021/acs.nanolett.3c02658>

## Author Contributions

<sup>†</sup>W.K. and S.Y.S. contributed equally.

## Notes

The authors declare no competing financial interest.

## ■ ACKNOWLEDGMENTS

Experimental measurements were supported by the U.S.  
Department of Energy, Office of Science, Materials Sciences  
and Engineering Division (W.K., P.M.). Experiments were  
carried out as part of the user project at the Center for  
Nanophase Materials Sciences, Oak Ridge National Labo-  
ratory, which is a U.S. Department of Energy Office of Science  
User Facility. J.L.L. acknowledges the computational resources  
provided by the Aalto Science-IT project and the financial  
support from the Academy of Finland Project No. 331342 and  
No. 336243 and the Jane and Aatos Erkkö Foundation.

## ■ REFERENCES

- (1) Bardeen, J.; Cooper, L. N.; Schrieffer, J. R. Theory of Superconductivity. *Phys. Rev.* **1957**, *108*, 1175–1204.
- (2) Tinkham, M. *Introduction to Superconductivity*, 2nd ed.; Dover Publications: New York, 2004.
- (3) Sigrist, M.; Ueda, K. Phenomenological theory of unconventional superconductivity. *Rev. Mod. Phys.* **1991**, *63*, 239–311.
- (4) Scalapino, D. J. A common thread: The pairing interaction for unconventional superconductors. *Rev. Mod. Phys.* **2012**, *84*, 1383–1417.
- (5) Kang, J.; Fernandes, R. M. Superconductivity in FeSe Thin Films Driven by the Interplay between Nematic Fluctuations and Spin-Orbit Coupling. *Phys. Rev. Lett.* **2016**, *117*, 217003.
- (6) Lederer, S.; Schattner, Y.; Berg, E.; Kivelson, S. A. Enhancement of Superconductivity near a Nematic Quantum Critical Point. *Phys. Rev. Lett.* **2015**, *114*, 097001.
- (7) Chowdhury, D.; Sachdev, S. Feedback of superconducting fluctuations on charge order in the underdoped cuprates. *Phys. Rev. B* **2014**, *90*, 134516.
- (8) Arpaia, R.; Ghiringhelli, G. Charge Order at High Temperature in Cuprate Superconductors. *J. Phys. Soc. Jpn.* **2021**, *90*, 111005.
- (9) Kreisel, A.; Hirschfeld, P. J.; Andersen, B. M. On the Remarkable Superconductivity of FeSe and Its Close Cousins. *Symmetry* **2020**, *12*, 1402.
- (10) Fernandes, R. M.; Coldea, A. I.; Ding, H.; Fisher, I. R.; Hirschfeld, P. J.; Kotliar, G. Iron pnictides and chalcogenides: a new paradigm for superconductivity. *Nature* **2022**, *601*, 35–44.
- (11) Hirschfeld, P. J.; Korshunov, M. M.; Mazin, I. I. Gap symmetry and structure of Fe-based superconductors. *Rep. Prog. Phys.* **2011**, *74*, 124508.

- 451 (12) Dai, P. Antiferromagnetic order and spin dynamics in iron-  
452 based superconductors. *Rev. Mod. Phys.* **2015**, *87*, 855–896.
- 453 (13) Livanas, G.; Aperis, A.; Kotetes, P.; Varelogiannis, G.  
454 Nematicity from mixed  $s_x + d_x^2 - y^2$  states in iron-based super-  
455 conductors. *Phys. Rev. B* **2015**, *91*, 104502.
- 456 (14) Kang, J.; Fernandes, R. M.; Chubukov, A. Superconductivity in  
457 FeSe: The Role of Nematic Order. *Phys. Rev. Lett.* **2018**, *120*, 267001.
- 458 (15) Kushnirenko, Y. S.; Fedorov, A. V.; Haubold, E.; Thirupathiah,  
459 S.; Wolf, T.; Aswartham, S.; Morozov, I.; Kim, T. K.; Büchner, B.;  
460 Borisenko, S. V. Three-dimensional superconducting gap in FeSe  
461 from angle-resolved photoemission spectroscopy. *Phys. Rev. B* **2018**,  
462 *97*, 180501.
- 463 (16) Kang, J.; Chubukov, A. V.; Fernandes, R. M. Time-reversal  
464 symmetry-breaking nematic superconductivity in FeSe. *Phys. Rev. B*  
465 **2018**, *98*, 064508.
- 466 (17) Islam, K. R.; Böker, J.; Eremin, I. M.; Chubukov, A. V. Specific  
467 heat and gap structure of a nematic superconductor: Application to  
468 FeSe. *Phys. Rev. B* **2021**, *104*, 094522.
- 469 (18) Sarma, S.; Freedman, M.; Nayak, C. Majorana zero modes and  
470 topological quantum computation. *npj Quantum Inf.* **2015**, *1*, 15001.
- 471 (19) Flensberg, K.; von Oppen, F.; Stern, A. Engineered platforms  
472 for topological superconductivity and Majorana zero modes. *Nat. Rev.*  
473 *Mater.* **2021**, *6*, 944–958.
- 474 (20) Sauls, J. A. Andreev bound states and their signatures.  
475 *Philosophical Transactions of the Royal Society A: Mathematical,*  
476 *Physical and Engineering Sciences* **2018**, *376*, 20180140.
- 477 (21) Kashiwaya, S.; Tanaka, Y.; Koyanagi, M.; Kajimura, K. Theory  
478 for tunneling spectroscopy of anisotropic superconductors. *Phys. Rev.*  
479 *B* **1996**, *53*, 2667–2676.
- 480 (22) Wei, J. Y. T.; Yeh, N.-C.; Garrigus, D. F.; Strasik, M.  
481 Directional Tunneling and Andreev Reflection on  $\text{YBa}_2\text{Cu}_3\text{O}_{7-\delta}$   
482 Single Crystals: Predominance of d-Wave Pairing Symmetry Verified  
483 with the Generalized Blonder, Tinkham, and Klapwijk Theory. *Phys.*  
484 *Rev. Lett.* **1998**, *81*, 2542–2545.
- 485 (23) Deutscher, G. Andreev–Saint-James reflections: A probe of  
486 cuprate superconductors. *Rev. Mod. Phys.* **2005**, *77*, 109–135.
- 487 (24) Daghero, D.; Tortello, M.; Ummarino, G. A.; Gonnelli, R. S.  
488 Directional point-contact Andreev-reflection spectroscopy of Fe-  
489 based superconductors: Fermi surface topology, gap symmetry, and  
490 electron–boson interaction. *Rep. Prog. Phys.* **2011**, *74*, 124509.
- 491 (25) Bashlakov, D. L.; Gamayunova, N. V.; Tyutrina, L. V.;  
492 Kačmarčík, J.; Szabó, P.; Samuely, P.; Naidyuk, Y. G. Sub-kelvin  
493 Andreev reflection spectroscopy of superconducting gaps in FeSe.  
494 *Low Temp. Phys.* **2019**, *45*, 1222–1226.
- 495 (26) Naidyuk, Y. G.; Kvitnitskaya, O. E.; Gamayunova, N. V.;  
496 Bashlakov, D. L.; Tyutrina, L. V.; Fuchs, G.; Hühne, R.; Chareev, D.  
497 A.; Vasiliev, A. N. Superconducting gaps in FeSe studied by soft point-  
498 contact Andreev reflection spectroscopy. *Phys. Rev. B* **2017**, *96*,  
499 094517.
- 500 (27) Cercellier, H.; Rodière, P.; Toulemonde, P.; Marcenat, C.;  
501 Klein, T. Influence of the quasiparticle spectral weight in FeSe on  
502 spectroscopic, magnetic, and thermodynamic properties. *Phys. Rev. B*  
503 **2019**, *100*, 104516.
- 504 (28) Ko, W.; Lado, J. L.; Maksymovych, P. Noncontact Andreev  
505 Reflection as a Direct Probe of Superconductivity on the Atomic  
506 Scale. *Nano Lett.* **2022**, *22*, 4042–4048.
- 507 (29) Song, C.-L.; Wang, Y.-L.; Jiang, Y.-P.; Wang, L.; He, K.; Chen,  
508 X.; Hoffman, J. E.; Ma, X.-C.; Xue, Q.-K. Suppression of  
509 Superconductivity by Twin Boundaries in FeSe. *Phys. Rev. Lett.*  
510 **2012**, *109*, 137004.
- 511 (30) Watashige, T.; Tsutsumi, Y.; Hanaguri, T.; Kohsaka, Y.;  
512 Kasahara, S.; Furusaki, A.; Sigrist, M.; Meingast, C.; Wolf, T.;  
513 Löhneysen, H. v.; Shibauchi, T.; Matsuda, Y. Evidence for Time-  
514 Reversal Symmetry Breaking of the Superconducting State near Twin-  
515 Boundary Interfaces in FeSe Revealed by Scanning Tunneling  
516 Spectroscopy. *Phys. Rev. X* **2015**, *5*, 031022.
- 517 (31) Song, S. Y.; Hua, C.; Bell, L.; Ko, W.; Fangohr, H.; Yan, J.;  
518 Halász, G. B.; Dumitrescu, E. F.; Lawrie, B. J.; Maksymovych, P.  
Nematically Templated Vortex Lattices in Superconducting FeSe. *519*  
*Nano Lett.* **2023**, *23*, 2822. 520
- (32) Hoffman, J. E.; McElroy, K.; Lee, D.-H.; Lang, K. M.; Eisaki, 521  
H.; Uchida, S.; Davis, J. C. Imaging Quasiparticle Interference in 522  
 $\text{Bi}_2\text{Sr}_2\text{CaCu}_2\text{O}_{8+\delta}$ . *Science* **2002**, *297*, 1148–1151. 523
- (33) Hanaguri, T.; Kohsaka, Y.; Davis, J. C.; Lupien, C.; Yamada, I.; 524  
Azuma, M.; Takano, M.; Ohishi, K.; Ono, M.; Takagi, H. 525  
Quasiparticle interference and superconducting gap in 526  
 $\text{Ca}_{2-x}\text{Na}_x\text{CuO}_2\text{Cl}_2$ . *Nat. Phys.* **2007**, *3*, 865–871. 527
- (34) Zou, C.; Hao, Z.; Luo, X.; Ye, S.; Gao, Q.; Xu, M.; Li, X.; Cai, 528  
P.; Lin, C.; Zhou, X.; Lee, D.-H.; Wang, Y. Particle–hole asymmetric 529  
superconducting coherence peaks in overdoped cuprates. *Nat. Phys.* 530  
**2022**, *18*, 551–557. 531
- (35) Chuang, T.-M.; Allan, M. P.; Lee, J.; Xie, Y.; Ni, N.; Bud'ko, S. 532  
L.; Boebinger, G. S.; Canfield, P. C.; Davis, J. C. Nematic Electronic 533  
Structure in the “Parent” State of the Iron-Based Superconductor 534  
 $\text{Ca}(\text{Fe}_{1-x}\text{Co}_x)_2\text{As}_2$ . *Science* **2010**, *327*, 181–184. 535
- (36) Allan, M. P.; Rost, A. W.; Mackenzie, A. P.; Xie, Y.; Davis, J. C.; 536  
Kihou, K.; Lee, C. H.; Iyo, A.; Eisaki, H.; Chuang, T.-M. Anisotropic 537  
Energy Gaps of Iron-Based Superconductivity from Intraband 538  
Quasiparticle Interference in  $\text{LiFeAs}$ . *Science* **2012**, *336*, 563–567. 539
- (37) Kostin, A.; Sprau, P. O.; Kreisel, A.; Chong, Y. X.; Böhmer, A. 540  
E.; Canfield, P. C.; Hirschfeld, P. J.; Andersen, B. M.; Davis, J. C. S. 541  
Imaging orbital-selective quasiparticles in the Hund’s metal state of 542  
FeSe. *Nat. Mater.* **2018**, *17*, 869–874. 543
- (38) Sukhachov, P. O.; von Oppen, F.; Glazman, L. I. Andreev 544  
Reflection in Scanning Tunneling Spectroscopy of Unconventional 545  
Superconductors. *Phys. Rev. Lett.* **2023**, *130*, 216002. 546
- (39) Lee, W.-C.; Park, W. K.; Arham, H. Z.; Greene, L. H.; Phillips, 547  
P. Theory of point contact spectroscopy in correlated materials. *Proc.* 548  
*Natl. Acad. Sci. U. S. A.* **2015**, *112*, 651–656. 549
- (40) Kulik, I. O.; Ellialtıoglu, R. *Quantum Mesoscopic Phenomena and* 550  
*Mesoscopic Devices in Microelectronics*; Kluwer Academic: Dordrecht, 551  
The Netherlands, 2000. 552
- (41) Miyata, Y.; Nakayama, K.; Sugawara, K.; Sato, T.; Takahashi, T. 553  
High-temperature superconductivity in potassium-coated multilayer 554  
FeSe thin films. *Nat. Mater.* **2015**, *14*, 775–779. 555
- (42) Wen, C. H. P.; Xu, H. C.; Chen, C.; Huang, Z. C.; Lou, X.; Pu, 556  
Y. J.; Song, Q.; Xie, B. P.; Abdel-Hafeez, M.; Chareev, D. A.; Vasiliev, 557  
A. N.; Peng, R.; Feng, D. L. Anomalous correlation effects and unique 558  
phase diagram of electron-doped FeSe revealed by photoemission 559  
spectroscopy. *Nat. Commun.* **2016**, *7*, 10840. 560
- (43) Wang, Q.-Y.; Li, Z.; Zhang, W.-H.; Zhang, Z.-C.; Zhang, J.-S.; 561  
Li, W.; Ding, H.; Ou, Y.-B.; Deng, P.; Chang, K.; Wen, J.; Song, C.-L.; 562  
He, K.; Jia, J.-F.; Ji, S.-H.; Wang, Y.-Y.; Wang, L.-L.; Chen, X.; Ma, X.- 563  
C.; Xue, Q.-K. Interface-Induced High-Temperature Superconductiv- 564  
ity in Single Unit-Cell FeSe Films on  $\text{SrTiO}_3$ . *Chin. Phys. Lett.* **2012**, 565  
*29*, 037402. 566
- (44) He, S.; et al. Phase diagram and electronic indication of high- 567  
temperature superconductivity at 65 K in single-layer FeSe films. *Nat.* 568  
*Mater.* **2013**, *12*, 605–610. 569
- (45) Wang, Z.; Zhang, P.; Xu, G.; Zeng, L. K.; Miao, H.; Xu, X.; 570  
Qian, T.; Weng, H.; Richard, P.; Fedorov, A. V.; Ding, H.; Dai, X.; 571  
Fang, Z. Topological nature of the  $\text{FeSe}_{0.5}\text{Te}_{0.5}$  superconductor. *Phys.* 572  
*Rev. B* **2015**, *92*, 115119. 573
- (46) Zhang, P.; Yaji, K.; Hashimoto, T.; Ota, Y.; Kondo, T.; 574  
Okazaki, K.; Wang, Z.; Wen, J.; Gu, G. D.; Ding, H.; Shin, S. 575  
Observation of topological superconductivity on the surface of an 576  
iron-based superconductor. *Science* **2018**, *360*, 182–186. 577
- (47) Qureshi, N.; Drees, Y.; Werner, J.; Wurmehl, S.; Hess, C.; 578  
Klingeler, R.; Büchner, B.; Fernández-Díaz, M. T.; Braden, M. Crystal 579  
and magnetic structure of the oxypnictide superconductor  $\text{LaFeAsO}_{1-x}\text{F}_x$ : 580  
A neutron-diffraction study. *Phys. Rev. B* **2010**, *82*, 184521. 581
- (48) Lebegue, S. Electronic structure and properties of the Fermi 582  
surface of the superconductor  $\text{LaOFeP}$ . *Phys. Rev. B* **2007**, *75*, 035110. 583
- (49) Fanfarillo, L.; Mansart, J.; Toulemonde, P.; Cercellier, H.; Le 584  
Fevre, P.; Bertran, F.; Valenzuela, B.; Benfatto, L.; Brouet, V. Orbital- 585  
dependent Fermi surface shrinking as a fingerprint of nematicity in 586  
FeSe. *Phys. Rev. B* **2016**, *94*, 155138. 587

588 (50) Balatsky, A. V.; Vekhter, I.; Zhu, J.-X. Impurity-induced states  
589 in conventional and unconventional superconductors. *Rev. Mod. Phys.*  
590 **2006**, *78*, 373–433.